Crashworthy Design of Composite Structures by CAE Process Chain

Madhukar Chatiri[1], Thorsten Schütz[2], Anton Matzenmiller[3]

[1]CADFEM GmbH, Grafing/Munich, Germany, mchatiri@cadfem.de
[2]Adam Opel AG, GME Vehicle CAE, Ruesselsheim, Germany, thorsten.schuetz@de.opel.com
[3]Institute of Mechanics, University of Kassel, Kassel, Germany, post-structure@uni-kassel.de

Summary

The materials used in automotive industry should play a key role in overcoming the current challenging demands such as increased global competition, need for vehicles with highest efficiency, reduction in costs, stringent environmental and safety requirements. This eventual usage of lighter materials means lighter vehicles and low greenhouse gas emissions. Composites are getting more recognition and, hence, being used increasingly in the automotive industry due to their excellent weight specific characteristics such as strength and stiffness. Thus, the requirements for the simulations along the complete production process chain involving reinforced plastics have increased immensely. The main objective of this paper is to present a workflow for numerical modeling and simulation of carbon fiber reinforced plastic composite structures including computer-aided engineering process integration. In this regard, a computational constitutive model for anisotropic damage is developed to characterize the elastic-brittle behavior of fiber-reinforced laminated composites. The presented work will introduce and discuss single steps along the process chain with in-house tools and the commercial finite element program LS-DYNA®.

Keywords: Carbon fiber-reinforced plastic, Computer-aided process chain, Composite damage model, Anisotropic damage, Analysis of multi-layered solid, First-ply failure, Puck's failure criteria

1 Introduction

In the present work, a computer-aided engineering (CAE) process chain is described for thick and thin composite structures which consists of two parts:

- generation of finite element (FE) input desk with fiber orientation and layer set-up,
- 3D explicit finite-element analysis (FEA) with (a) Multi-layered solid/multi-layered shell elements and (b) a constitutive model wherein the damage initiation criteria are based on Puck's model for first ply failure and the progressive micro crack propagation relies on continuum damage evolution.

2 CAE process chain

The various manufacturing technologies of carbon fiber-reinforced plastic (CFRP) composite structures have to be represented in the finite element simulations in order to capture possible failure events during the production process and exactly map the fiber orientations into the FE input deck. The CAE tool chain, presented in [1], captures the above mentioned phenomena in manufacturing of thick composite structures (three dimensional stress state) and thin ones (two-dimensional stress state), and is explained here.

High pressure hydrogen storage systems (HSSs) for fuel cell vehicles with an operating pressure of 70 MPa are made of CFRP laminates with a wall thickness of 40 mm to 60 mm. Here, three aspects are important. Firstly, the vessel has to fit into the given package space of the vehicle. Secondly, the vessel has to withstand a certain inner pressure and third, the vessel plus integration features have to pass certain vehicle crash acceptance criteria. Thus, it is necessary to integrate the high pressure vessel into standard CAE processes in order to work on these aspects in the early phase of a fuel cell vehicle development. The aspect of data importing/exporting interface between individual tools, especially between the wet-winding process simulation and the FEA tools is quite efficiently done in the current tool chain (see Fig. 1).

The starting point in the vessel pre-dimensioning phase is the given package envelope of the vehicle. This envelope defines the maximum outer dimensions of the vessel at the maximum allowable working pressure. In the next step, the nominal outer dimensions of the vessel are determined using an estimation

Netting theory and CLT	PyWind	ANSYS Composite PrepPost	LS-DYNA®
Design of the cylindrical part of the vessel	Virtual manufacturing of the vessel	Generation of a FE model of the vessel	FE model of the HSS module
① →	② →	③ →	④
Classical laminate theory	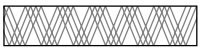	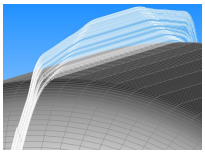	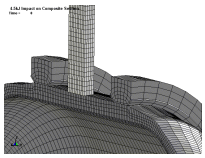

Fig. 1: CAE process chain for thick walled composite structures.

of the expansion of the vessel under pressure. An iterative process is applied to determine the required number of helical and hoop layers, the starting winding angle and the thickness of the composite. The whole iterative process considers just the cylindrical part of the vessel assuming a two-dimensional state of stress and applies netting theory and classical laminate theory in a subsequent manner.

In the third step, the PyWind data is imported inside ANSYS Composite PrepPost (ACP) and a detailed multi-layered solid finite element mesh of the wet wound composite vessel is generated. The solid FE mesh generated from ACP is *ELEMENT_TSHELL_COMPOSITE [2] which allows a very comfortable description of composite layers using a ply-based concept. The FE solid model consists of a multi-layered solid element (TSHELL type 5) which resolves the 3D stress state necessary for impact directions normal to the outer vessel surface. Also this element allows the definition of multiple integration points through the thickness in order to account for stacks of plies with arbitrary fiber orientation. In the final step, impact and crash simulation models are generated inside LS-PrePost and simulations are done using LS-DYNA®.

The CAE process chain, developed for thick composite structures, is adapted to thin shell applications. The thin shell composite draping simulation is done using FiberSim, whose data is imported inside ACP to build the composite shell structure (see Fig. 2). The output of the FE mesh is *ELEMENT_SHELL_COMPOSITE [2] which allows a very comfortable description of composite layers using a ply-based concept. Also the three dimensional material model is adapted to thin shell structures.

Netting theory and CLT	FiberSim	ANSYS Composite PrepPost	LS-DYNA®
Design/definition of composite shell	Draping simulation	Generation of a FE model	FE model of thin shell component
① →	② →	③ →	④
Classical laminate theory	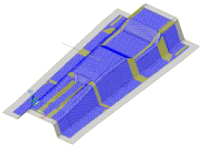	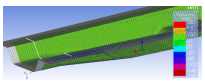	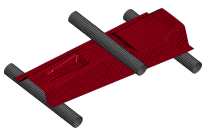

Fig. 2: CAE process chain for thin walled composite structures.

3 Constitutive modeling of composite structures

A computational constitutive model for anisotropic damage is developed to characterize the elastic-brittle behavior of fiber-reinforced laminated composites. The composite damage model is implemented within

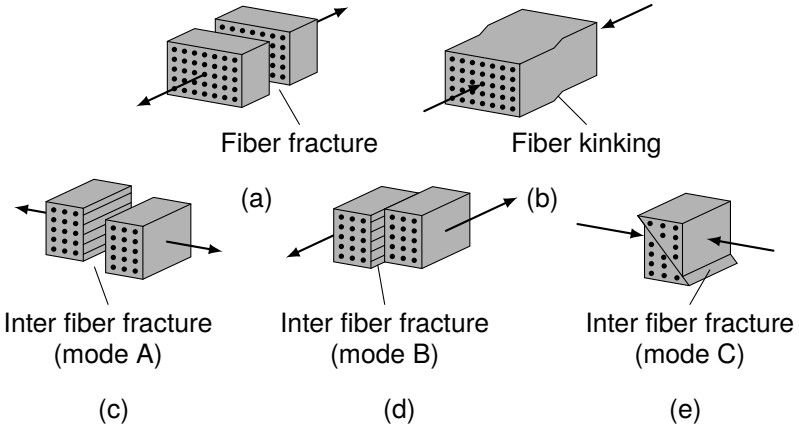

Fig. 3: Major failure modes considered in the model as in [4].

LS-DYNA® [2] as a user defined material subroutine which can describe progressive failure and damage behavior of CFRP composites [3]. A homogenized continuum is adopted for the constitutive theory of anisotropic damage and elasticity. Damage initiation criteria or first ply failure prediction is based on the Puck's failure criteria [4, 5] and progressive damage is based on continuum damage mechanics [6]. Internal variables are introduced to describe the evolution of the damage state under loading and as a consequence the degradation of the material stiffness occurs. The corresponding rate equations are subjected to laws of thermomechanics. Emphasis is placed on a suitable coupling among the equations for the rates of the damage variables with respect to different damage modes. The integrated routine is successfully utilized to predict failure and damage of composite laminates which are subjected to impact conditions.

3.1 Fiber failure (FF) or longitudinal failure

Fiber fracture, see Fig. 3 (a) and (b), is primarily caused by the stress σ_{11} which acts parallel to the fibers. It expresses the physical idea that fiber fracture under a multiaxial state of stress in a UD-lamina occurs when its stress parallel to the fibers σ_{11} is equal to or exceeds the stress necessary for fracture. The simple Puck FF-condition follows from this hypothesis [7, 4, 5]. It describes by case distinction the tensile fiber mode $f^{+}_{\mathrm{E,FF}}$ for $\sigma_{11} \geq 0$:

$$f^{+}_{\mathrm{E,FF}} = \left(\frac{\sigma_{11}}{R^{+}_{\parallel}}\right)^{2} - 1 \quad \begin{cases} \geq 0 & \text{failed} \\ < 0 & \text{elastic} \end{cases} \tag{1}$$

and the compressive fiber mode $f^{-}_{\mathrm{E,FF}}$ for $\sigma_{11} < 0$:

$$f^{-}_{\mathrm{E,FF}} = \left(\frac{\sigma_{11}}{R^{-}_{\parallel}}\right)^{2} - 1 \quad \begin{cases} \geq 0 & \text{failed} \\ < 0 & \text{elastic} \end{cases} \tag{2}$$

wherein $R^{+}_{\parallel}$, $R^{-}_{\parallel}$ denote the corresponding material strength parameters.

3.2 Inter fiber failure (IFF) or transverse failure

Normal stresses, acting transverse to the fibers and shear stresses are transmitted through both matrix and fibers. However, their damaging effect mainly takes place in the matrix or in the fiber-matrix interface, leading to debonding. Usually, the bond strength of the interface zone between fibers and matrix is the lowest in comparison to the data for the strength of the single constituents. Advancing cracks in the matrix soon pass into the fiber-matrix interface and propagate along the fibers without crossing into the fiber material. Progressive opening of existing cracks is characteristic for tensile loading in transverse direction, whereas "crushing" in the sense of "fragmentation" of brittle matrix materials is very typical for compression in transverse direction. Following the inter fiber failure (IFF) observations outlined above, the failure modes considered in the model are schematically represented in Fig. 3 (c), (d), and (e).

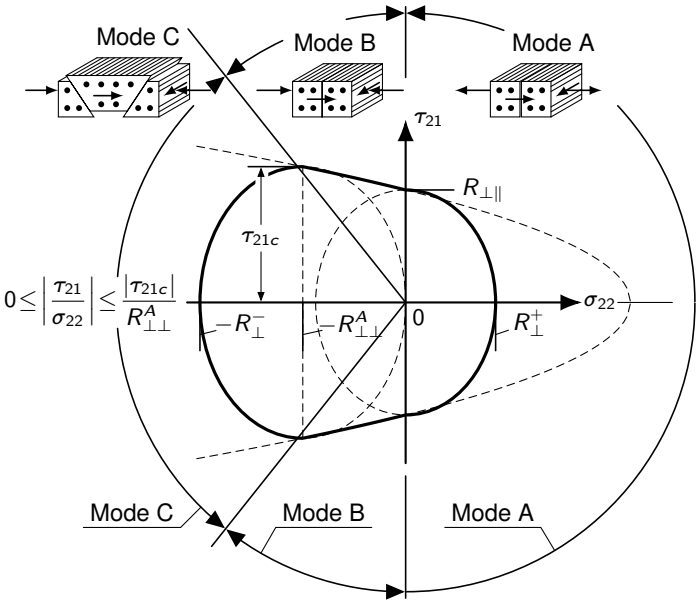

Fig. 4: Schematic representation of failure modes and failure plane based on Puck's model [5].

For the above described transverse failure, the Puck IFF criteria are most promising for brittle, plastic unidirectional (UD-)laminates, see Fig. 4. The UD-ply behaves transversely isotropic in both cases, elasticity and failure. Puck assumes a Mohr-Coulomb type of failure criterion for loading transverse to the fiber direction. Failure is assumed to be caused by the normal and shear components operating on the action plane [7] of stresses σ_n, τ_{n1}, τ_{nt}, see Fig. 4. Positive normal stress on this plane promotes fracture while a negative one increases the material's shear strength, thus, impeding fracture. Puck's stress based failure criteria enable the computation of the material exposure $f_{\mathrm{E,IFF}}(\theta)$ as a failure indicator, wherein θ is the orientation angle. The three-dimensional Puck's failure criteria can be categorized as below in Tab. 1 in extension to Fig. 4.

Tab. 1: Categorization of fracture modes in failure criteria of Puck under three-dimensional stress states.

Fracture angle	**Sign of σ_n**	**Fracture mode**
90°	positive	Delamination
0° to 89°	positive	A
−53° to 0°	negative	B
−90° to −53°	negative	C

The values of inter fiber failure in tension $f^+_{\mathrm{E,IFF}}(\theta)$ and the same for compression $f^-_{\mathrm{E,IFF}}(\theta)$ range between zero, where the material is unstressed, and up to one, denoting the onset of inter fiber failure. The master failure surface on the fracture plane is defined in terms of the stress components acting on the fracture plane denoted here as Mohr-Coulomb stresses. Thus, yielding the following inter fiber failure criteria by case distinction in tension and compression, for $\sigma_n \geq 0$:

$$f^+_{\mathrm{E,IFF}}(\theta) = \sqrt{\left[\frac{1}{R^+_\perp} - \frac{p^+_{\perp\psi}}{R^A_{\perp\psi}}\right]^2 \sigma_n^2(\theta) + \left[\frac{\tau_{nt}(\theta)}{R^A_{\perp\perp}}\right]^2 + \left[\frac{\tau_{n1}(\theta)}{R_{\perp\parallel}}\right]^2} + \frac{p^+_{\perp\psi}}{R^A_{\perp\psi}}\sigma_n(\theta) - 1 \tag{3}$$

and for $\sigma_n < 0$:

$$f^-_{\mathrm{E,IFF}}(\theta) = \sqrt{\left[\frac{\tau_{nt}(\theta)}{R^A_{\perp\perp}}\right]^2 + \left[\frac{\tau n1(\theta)}{R_{\perp\parallel}}\right]^2 + \left[\frac{p^-_{\perp\psi}}{R_{\perp\psi}}\sigma_n(\theta)\right]^2} + \frac{p^-_{\perp\psi}}{R^A_{\perp\psi}}\sigma_n(\theta) - 1 \tag{4}$$

The only unknown parameters in these equations are $p^\pm_{\perp\psi}$, $R^A_{\perp\psi}$, and $R^A_{\perp\perp}$ which depend on the shear

stresses τ_{nt} and τ_{n1} according to the following equations:

$$\frac{p^{\pm}_{\perp\psi}}{R^{A}_{\perp\psi}} = \frac{p^{\pm}_{\perp\perp}}{R^{A}_{\perp\perp}} \frac{\tau^2_{nt}}{\tau^2_{nt}+\tau^2_{n1}} + \frac{p^{\pm}_{\perp\parallel}}{R_{\perp\parallel}} \frac{\tau^2_{n1}}{\tau^2_{nt}+\tau^2_{n1}} \quad \text{and} \quad R^{A}_{\perp\perp} = \frac{R^{-}_{\perp}}{2(1+p^{-}_{\perp\perp})} \tag{5, 6}$$

wherein $R^{+}_{\perp}$, $R_{\perp\parallel}$, $R^{-}_{\perp}$ denote the corresponding material strength parameters, and $p^{\pm}_{\perp\perp}$, $p^{\pm}_{\perp\parallel}$ are constants introduced by PUCK, see [5]. The action plane with the greatest failure effort $f_{\mathrm{E}}(\theta)$, where $\theta = -90°$ to $90°$ is the fracture plane to be expected, $f_{\mathrm{E}}|_{\theta=\theta_{\mathrm{fp}}} := [f_{\mathrm{E}}(\theta)]_{\max}$. Once the failure plane with maximal $f_{\mathrm{E}}(\theta)$ is found, the fracture angle as θ_{fp} is kept constant in the model and progressive failure, based on the idea of continuum damage, is applied to the material model for the corresponding lamina at hand, see below.

3.3 Damage evolution and stiffness degradation

The failure criteria may be interpreted as loading criteria, a terminology encountered in strain space plasticity. The role played by the yield stress in plasticity will be taken by the threshold variables r_i in damage mechanics. In classical continuum damage mechanics, only the undamaged (whole) part of the cross-section A (net-area) for the uniaxial case is supposed to carry loading, i.e. transmit stresses. Consequently, the stresses σ_{ij} in the failure criteria should be interpreted as effective stresses $\hat{\sigma}_{ij}$, referred to the net area. This means that the failure criteria are assumed to hold in terms of the effective stresses rather than the nominal ones.

If the degradation is described in the sense of CAUCHY's stress concept, six different non-negative damage parameters ω_{11}, ω_{22}, ω_{33}, ω_{12}, ω_{23} and ω_{13} are defined to quantify the relative size of diffused cracks projected onto the coordinate planes, and assembled in the rank-four damage operator $\mathbf{M}$ given in VOIGT notation of Eq. (8d). In continuum damage mechanics (CDM), the effective normal stresses $\hat{\boldsymbol{\sigma}}$ are related to the damage parameters ω_{ij}, since only the undamaged part of the cross section A for the uniaxial case is supposed to carry loading. Consequently, the stresses σ_{ij} in the failure criteria should be interpreted as effective stresses $\hat{\sigma}_{ij}$, referred to the net area. A simple relationship between effective stress $\hat{\boldsymbol{\sigma}}$ and the nominal one $\boldsymbol{\sigma}$ holds:

$$\hat{\boldsymbol{\sigma}} = \mathbf{M}\boldsymbol{\sigma} \tag{7}$$

wherein $\mathbf{M}$ represents the rank-four (uncoupled) damage operator given in VOIGT notation as:

$$\boldsymbol{\sigma} = \begin{bmatrix} \sigma_{11} \\ \sigma_{22} \\ \sigma_{33} \\ \tau_{12} \\ \tau_{23} \\ \tau_{13} \end{bmatrix}, \quad \hat{\boldsymbol{\sigma}} = \begin{bmatrix} \hat{\sigma}_{11} \\ \hat{\sigma}_{22} \\ \hat{\sigma}_{33} \\ \hat{\tau}_{12} \\ \hat{\tau}_{23} \\ \hat{\tau}_{13} \end{bmatrix}, \quad \boldsymbol{\omega} = \begin{bmatrix} \omega_{11} \\ \omega_{22} \\ \omega_{33} \\ \omega_{12} \\ \omega_{23} \\ \omega_{13} \end{bmatrix}, \quad \mathbf{M} = \begin{bmatrix} \frac{1}{1-\omega_{11}} & 0 & 0 & 0 & 0 & 0 \\ 0 & \frac{1}{1-\omega_{22}} & 0 & 0 & 0 & 0 \\ 0 & 0 & \frac{1}{1-\omega_{33}} & 0 & 0 & 0 \\ 0 & 0 & 0 & \frac{1}{1-\omega_{12}} & 0 & 0 \\ 0 & 0 & 0 & 0 & \frac{1}{1-\omega_{23}} & 0 \\ 0 & 0 & 0 & 0 & 0 & \frac{1}{1-\omega_{13}} \end{bmatrix} \tag{8a–d}$$

In the undamaged state, a lamina behaves equally in the transverse 2-direction and the through-thickness 3-direction which allows reducing the general anisotropy to a transversely isotropic behavior with only a fiber-parallel $\parallel$ (1) and fiber-perpendicular $\perp$ (2) direction. The constitutive behavior, i.e. the material equation relating, states of stress to states of strain, is then defined by the transversely isotropic compliance matrix $\mathbf{S}$ in VOIGT notation for the UD-laminae prior to the damage initiation, see Eq. (9). The nonlinear behavior of in-plane shear is modeled by the shear stiffness G_{12} as a function of $\hat{G}_{12}$ of shear strain ϵ_{12}.

$$\begin{bmatrix} \epsilon_{11} \\ \epsilon_{22} \\ \epsilon_{33} \\ 2\epsilon_{12} \\ 2\epsilon_{23} \\ 2\epsilon_{13} \end{bmatrix} = \begin{bmatrix} 1/E_{11} & -\nu_{21}/E_{22} & -\nu_{31}/E_{33} & 0 & 0 & 0 \\ -\nu_{12}/E_{11} & 1/E_{22} & -\nu_{32}/E_{33} & 0 & 0 & 0 \\ -\nu_{13}/E_{11} & -\nu_{23}/E_{22} & 1/E_{33} & 0 & 0 & 0 \\ 0 & 0 & 0 & 1/\hat{G}_{12}(\epsilon_{12}) & 0 & 0 \\ 0 & 0 & 0 & 0 & 1/G_{23} & 0 \\ 0 & 0 & 0 & 0 & 0 & 1/G_{13} \end{bmatrix} \begin{bmatrix} \sigma_{11} \\ \sigma_{22} \\ \sigma_{33} \\ \sigma_{12} \\ \sigma_{23} \\ \sigma_{13} \end{bmatrix} \tag{9}$$

The components of the constitutive tensor $\mathbf{H}(\boldsymbol{\omega})$ for the deteriorated material are represented as functions of the vector $\boldsymbol{\omega}$, comprising all internal damage variables, and the material parameters of the undamaged lamina. The constitutive tensor $\mathbf{C}(\boldsymbol{\omega})$ is derived by physical arguments and information of the dependencies between effective elastic properties and individual damage variables. Generally, for a given arbitrary damage operator, the postulate of strain equivalence yields an unsymmetrical constitutive tensor, which should be rejected as a model for the elastic behavior. This hypothesis serves here as a first guidance together with physical arguments to set up the constitutive tensor $\mathbf{C}(\boldsymbol{\omega})$ for the damaged lamina. The compliance relationship for orthotropic elasticity in terms of effective stresses $\hat{\boldsymbol{\sigma}}$ reads as:

$$\boldsymbol{\epsilon} = \mathbf{H}_0\hat{\boldsymbol{\sigma}},\ \mathbf{H}_0 = \begin{bmatrix} 1/E_{11} & -\nu_{21}/E_{22} & -\nu_{31}/E_{33} & 0 & 0 & 0 \\ -\nu_{12}/E_{11} & 1/E_{22} & -\nu_{32}/E_{33} & 0 & 0 & 0 \\ -\nu_{13}/E_{11} & -\nu_{23}/E_{22} & 1/E_{33} & 0 & 0 & 0 \\ 0 & 0 & 0 & 1/\hat{G}_{12}(\epsilon_{12}) & 0 & 0 \\ 0 & 0 & 0 & 0 & 1/G_{23} & 0 \\ 0 & 0 & 0 & 0 & 0 & 1/G_{13} \end{bmatrix},\ \boldsymbol{\epsilon} = \begin{bmatrix} \epsilon_{11} \\ \epsilon_{22} \\ \epsilon_{33} \\ 2\epsilon_{12} \\ 2\epsilon_{23} \\ 2\epsilon_{13} \end{bmatrix} \tag{10a–c}$$

It is noted that Eq. (10b) is symmetric. Equations (7) and (10a) result in:

$$\boldsymbol{\epsilon} = \mathbf{H}_0\hat{\boldsymbol{\sigma}} = \mathbf{H}_0\mathbf{M}\boldsymbol{\sigma} \tag{11}$$

The final relationship of the compliance tensor for the damaged lamina $\mathbf{H}(\boldsymbol{\omega})$ takes the following form after Poisson's ratios $\nu_{12}(\boldsymbol{\omega})$, $\nu_{21}(\boldsymbol{\omega})$, $\nu_{13}(\boldsymbol{\omega})$, $\nu_{31}(\boldsymbol{\omega})$, $\nu_{23}(\boldsymbol{\omega})$, and $\nu_{32}(\boldsymbol{\omega})$ are adjusted according to the qualitative arguments presented in [6].

$$\mathbf{H}(\boldsymbol{\omega}) = \begin{bmatrix} \frac{1}{(1-\omega_{11})E_{11}} & -\frac{\nu_{21}}{E_{22}} & -\frac{\nu_{31}}{E_{33}} & 0 & 0 & 0 \\ -\frac{\nu_{12}}{E_{11}} & \frac{1}{(1-\omega_{22})E_{22}} & -\frac{\nu_{32}}{E_{33}} & 0 & 0 & 0 \\ -\frac{\nu_{13}}{E_{11}} & -\frac{\nu_{23}}{E_{22}} & \frac{1}{(1-\omega_{33})E_{33}} & 0 & 0 & 0 \\ 0 & 0 & 0 & \frac{1}{(1-\omega_{12})\hat{G}_{12}(\epsilon_{12})} & 0 & 0 \\ 0 & 0 & 0 & 0 & \frac{1}{(1-\omega_{23})G_{23}} & 0 \\ 0 & 0 & 0 & 0 & 0 & \frac{1}{(1-\omega_{13})G_{13}} \end{bmatrix} \tag{12}$$

The six components of the damage vector are not independent. In the concept of damage modes, these variables account for stiffness degradation due to fiber failure and inter fiber failure, see [3]. As explained earlier, the orthotropic nature of the lamina as a homogenized continuum is maintained throughout the damaging process. The shear coupling terms are neglected. Therefore, the symmetry class of the UD-lamina remains the same for all states of damage. Its inverse always exits as long as the damage variables are less than one ($\omega_{ij} < 1$). Hence, the material stiffness tensor is given by:

$$\mathbf{C}(\boldsymbol{\omega}) = [\mathbf{H}(\boldsymbol{\omega})]^{-1} \tag{13}$$

In the presence of strain softening, the rate of evolution for the damage $\dot{\boldsymbol{\omega}}(\boldsymbol{\sigma}, \boldsymbol{\omega}, \dot{\boldsymbol{\epsilon}})$ is supposed to be locally controllable under the strain rate $\dot{\boldsymbol{\epsilon}}$. Under these conditions, the rate-equations are:

$$\dot{\boldsymbol{\omega}} = \sum_i \varphi_i \mathbf{q}_i = \varphi_1\mathbf{q}_1 + \varphi_2\mathbf{q}_2 \tag{14}$$

The scalar functions $\varphi_i(\boldsymbol{\sigma}, \boldsymbol{\omega}, \dot{\boldsymbol{\epsilon}})$ are multiple damage functions which control the amount of growth and the vector-valued functions $\mathbf{q}_i(\boldsymbol{\sigma}, \boldsymbol{\omega})$ represent multiple damage coupling vectors which accommodate the coupling of growth for the individual damage variables in the various damage modes. Also, φ_i must be linear in $\dot{\boldsymbol{\epsilon}}$ for a rate-independent process, see [6].

In the softening range of post critical stress states, the damage growth functions φ_i can be obtained in the form of

$$\Phi_i = \int_0^t \varphi_i \, \mathrm{d}\bar{t} = 1 - \mathrm{e}^{\frac{1}{m_i}(1-[r_i]^{m_i})}, \quad r_i \geq 1 \tag{15}$$

where m_i is the strain softening parameter and r_i is the damage threshold for the criterion g_i at hand which can be expressed as the ratio between current total strain and corresponding yield strain.

$$r = \frac{\epsilon}{\epsilon_y} \tag{16}$$

3.4 Verification example

In this verification example, a tension test under loading transverse to the fiber direction on a UD-reinforced laminated composite is presented. The lamina material properties for elasticity are: $E_{11} = 126\,\text{GPa}$, $E_{22} = 11\,\text{GPa}$, $E_{33} = 11\,\text{GPa}$, $\nu_{12} = 0.28$, $\nu_{23} = 0.40$, $\nu_{13} = 0.28$, $G_{12} = 9\,\text{GPa}$; and for strength: $R_{\perp}^{+} = 45\,\text{MPa}$, $R_{\perp\parallel} = 79\,\text{MPa}$, $R_{\parallel}^{+} = 1950\,\text{MPa}$. The load is applied in transverse to the fiber direction until complete failure. Fig. 5 represents the evolution of damage variables in both the original two-dimensional (2D) model and the current three-dimensional (3D) extension of the model for the strain softening exponent $m = 1.0$. The original two-dimensional model from [6] is implemented as *MAT_058 in [2]. Here, the damage variables effect the stress-strain curves over the entire strain range. In the current model, the damage variables are only applicable to the post-failure part according to Eq. (15).

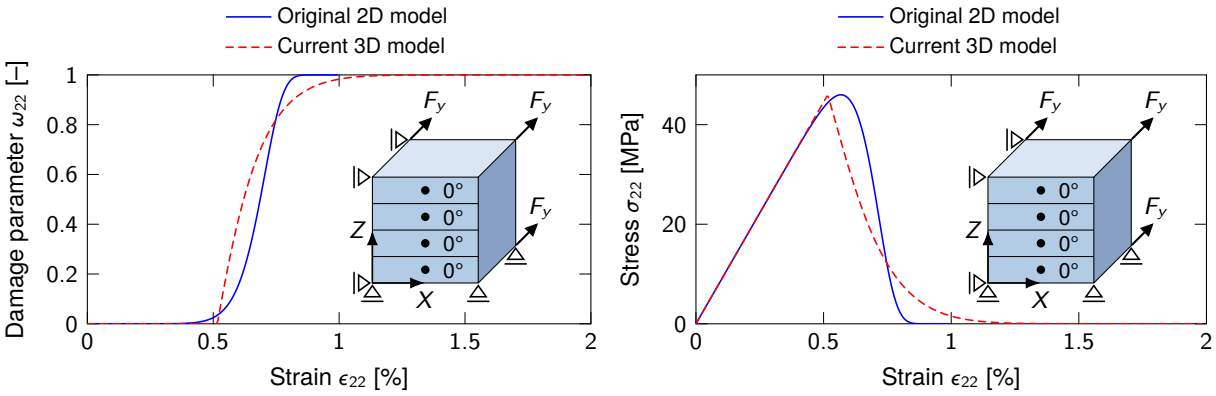

Fig. 5: Left: evolution of damage variable ω_{22} in the original 2D model and current 3D model and right: transverse stress-strain curve in both the models.

3.5 Comparison with existing material models of LS-DYNA®

The current user-defined constitutive approach is also tested and compared to existing material models MAT_022, MAT_054, and MAT_055, available within LS-DYNA®, see Fig. 6 and [2]. Here in this example, a tensile force transverse to the fiber direction is applied on a UD-reinforced laminated composite cube. The lamina material properties for elasticity are: $E_{11} = 126\,\text{GPa}$, $E_{22} = 11\,\text{GPa}$, $E_{33} = 11\,\text{GPa}$, $\nu_{12} = 0.28$, $\nu_{23} = 0.40$, $\nu_{13} = 0.28$, $G_{12} = 9\,\text{GPa}$; and for strength: $R_{\perp}^{+} = 45\,\text{MPa}$, $R_{\perp\parallel} = 79\,\text{MPa}$, $R_{\parallel}^{+} = 1950\,\text{MPa}$.

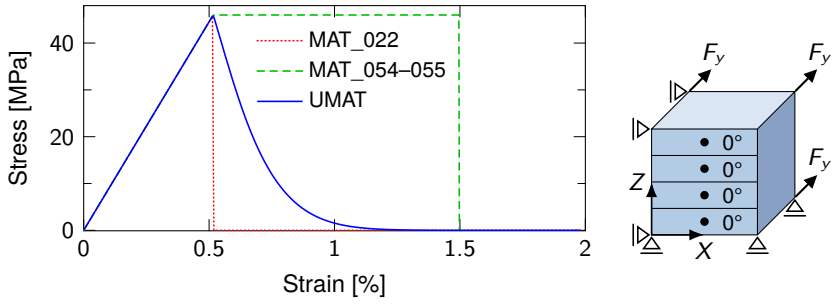

Fig. 6: Comparison of stresses from material models within LS-DYNA®.

3.6 Four-point bending of a thick composite structure

A four-point bending response on a laminate with configuration of $(\pm 20°_2/90°_4/\pm 20°_2/90°_4)$ is shown in the example below. The material properties are taken from [8]: $E_1 = 135\,718$ MPa, $E_2 = 8907$ MPa, $E_3 = 8907$ MPa, $G_{12} = 6281$ MPa, $\nu_{12} = 0.19$, $R_{\parallel}^{+} = 2187$ MPa, $R_{\parallel}^{-} = 991$ MPa, $R_{\perp}^{+} = 46$ MPa, $R_{\perp}^{-} = 155$ MPa, $R_{\perp\parallel} = 96$ MPa, $p_{\perp\parallel}^{+} = 0.43$, $p_{\perp\parallel}^{-} = 0.34$, $p_{\perp\perp}^{+} = 0.13$, $p_{\perp\perp}^{-} = 0.13$, $m = 0.5$, and $s = 0.5$. The thickness of each single unidirectional ply is 0.25 mm. The geometry and loading conditions are represented in Fig. 7.

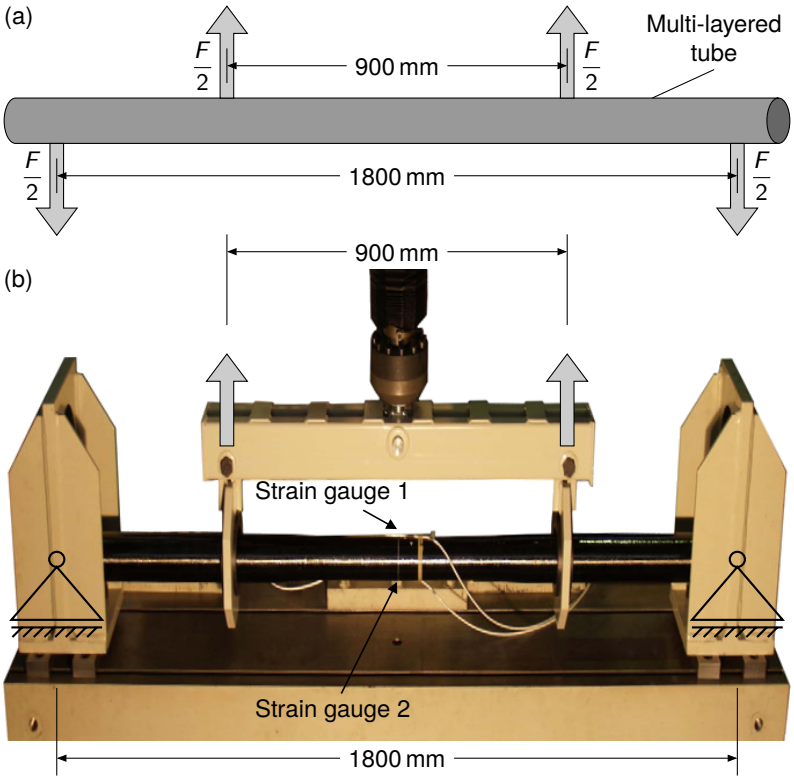

Fig. 7: Schematic picture of the loading case for four-point bending test on a multi-layered tube [8].

The simulated part is a quarter symmetry model. Fig. 8 (left) shows the IFF predicted by Pucк's failure criteria and Fig. 8 (right) shows the force vs. strain results compared with the experimental data. First inter fiber failure is detected in the 90° ply at a force of 17 kN, whereas it is 19 kN in the experiment. Delamination is detected when θ_{fp} is 90° and computation is stopped at a force level of 29 kN. In experiment, delamination is detected at 26 kN.

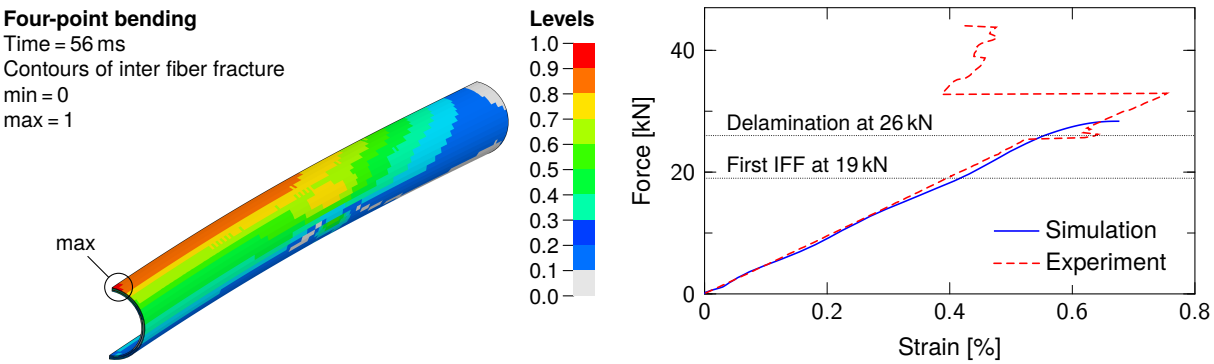

Fig. 8: Left: first-ply failure (IFF) inside the tube using 3D Pucк's failure criteria and right: comparison with test (strain gauge signal from tension side).

3.7 Three-point bending of a thin shell structure

To check the application of the developed material model to thin shell structures, a three-point bending simulation is performed on a hat profile with laminate configuration $(0°/90°/-45°/45°)_s$. The material properties are taken from [8]: $E_1 = 135\,718$ MPa, $E_2 = 8907$ MPa, $E_3 = 8907$ MPa, $G_{12} = 6281$ MPa, $\nu_{12} = 0.19$, $R_{\parallel}^{+} = 2187$ MPa, $R_{\parallel}^{-} = 991$ MPa, $R_{\perp}^{+} = 46$ MPa, $R_{\perp}^{-} = 155$ MPa, $R_{\perp\parallel} = 96$ MPa, $p_{\perp\parallel}^{+} = 0.43$, $p_{\perp\parallel}^{-} = 0.34$, $p_{\perp\perp}^{+} = 0.13$, $p_{\perp\perp}^{-} = 0.13$, $m = 0.5$, and $s = 0.5$. The thickness of each single unidirectional ply is 0.25 mm. The geometry and loading conditions are represented in Fig. 9.

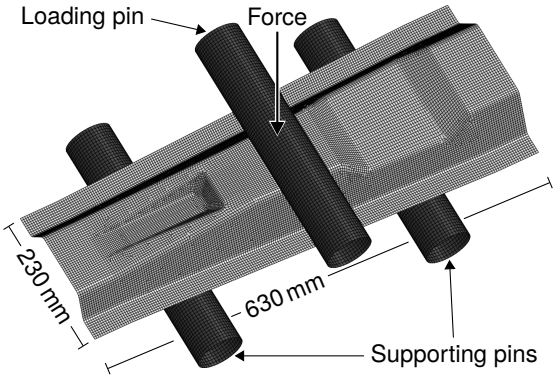

Fig. 9: Three-point bending test set-up of a thin shell structure.

Matrix damage is shown in Fig. 10, and force vs. displacement curve is plotted in Fig. 11. These simulation results will be compared with the experimental results in future. By using the history variables of the correspondent material model, the individual laminate loading and the correspondent damage states can be verified. For user defined material model, the damage variables “damage fiber compression and damage transverse direction” depict well the damaged areas. The damage variable “damage in transverse direction” shows the developed material model depicts a better resolution of the laminate effort and can be used as an indicator for delamination prediction and tendency.

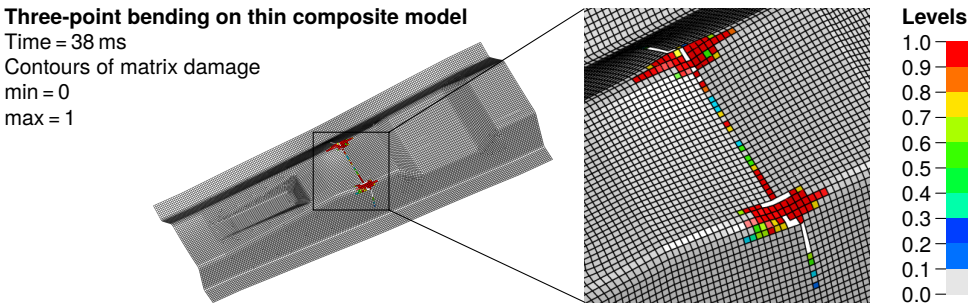

Fig. 10: Three-point bending test simulation results: Matrix damage distribution.

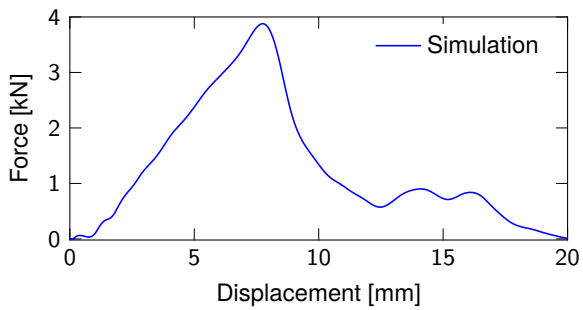

Fig. 11: Three-point bending test simulation results: Force vs. displacement curve.

4 Summary and conclusions

The CAE process chain is successfully implemented in the design phase both for thick as well as thin composite structures. The meso-level model with the 3D Puck's failure criteria and anisotropic continuum damage mechanics is very effective in analyzing multi-layered structures having a large number of plies. The developed material model describes both onset and progression of damage. It can reproduce the key physical aspects observed in the failure process of fiber-reinforced laminated composite structures.

Literature

[1] M. Chatiri and T. Schütz. "Optimized design of composite structures using CAE process chain". In: *Seminar: Simulation of composites – a closed process chain?* Leipzig, Germany: NAFEMS, Oct. 28, 2014.

[2] J. O. Hallquist et al. *LS-DYNA keyword manual version 971*. Livermore: Livermore Software Technology Corporation, 2013.

[3] M. Chatiri and A. Matzenmiller. "A damage-mode based three dimensional constitutive model for fibre-reinforced composites". In: *Computers, Materials and Continua* 35.3 (2013), pp. 255–283.

[4] M. Knops. *Analysis of failure in fibre polymer laminates: the theory of Alfred Puck*. Springer-Verlag: Berlin, Heidelberg, July 31, 2008. 205 pp.

[5] A. Puck and H. Schürmann. "Failure analysis of FRP laminates by means of physically based phenomenological models". In: *Failure criteria in fibre-reinforced-polymer composites*. Oxford: Elsevier, 2004. Chap. 5.6, pp. 832–876.

[6] A. Matzenmiller, J. Lubliner, and R. L. Taylor. "A constitutive model for anisotropic damage in fiber-composites". In: *Mechanics of Materials* 20.2 (Apr. 1995), pp. 125–152.

[7] Z. Hashin. "Failure criteria for unidirectional fiber composites". In: *Journal of Applied Mechanics* 47.2 (June 1, 1980), pp. 329–334.

[8] A. Bleier and H. Schurmann. *Establishment of a process for quasistatic dimensioning of a H_2 high-pressure vessel*. Internal report to Adam Opel GmbH, GM Fuel Cell Activities. KLuB TU Darmstadt, 2008. Sent via confidential email from Mr. T. Güll to M. Chatiri, CADFEM GmbH.